Roman Bruch*, Mario Vitacolonna, Rüdiger Rudolf, and Markus Reischl

Prediction of Fluorescent Ki67 Staining in 3D Tumor Spheroids

Abstract: 3D cell culture models are important tools for the development and testing of new therapeutics. In combination with immunoassays and 3D confocal microscopy, crucial information like morphological or metabolic changes can be examined during drug testing. However, a common limitation of immunostainings is the number of dyes that can be imaged simultaneously, as overlaps in the spectral profiles of the different dyes may result in cross talk.

We therefore present a 3D deep learning method, able to predict fluorescent stainings of specific antigens on the basis of a nuclei staining. Using the proliferation marker Ki67, we showed that the presented model was able to predict the Ki67 staining with a strong correlation to the real signal. Additional analysis showed, that the model was not relying on signal cross talk. This approach, based on staining of the cell nuclei and subsequent prediction of the target antigen, could reduce the number of parallel antigen stains to a minimum and incompatible staining panels could be circumvented in the future.

Keywords: Label Synthesis, 3D, Fluorescence Microscopy, Deep Learning, Ki67 Prediction.

1 Introduction

The development of new therapeutics is an important field of research in the medical sector. Cell culture models represent an essential platform for their testing. They allow the preclinical testing of substances and can provide vital information about the specificity of their effect.

New methods enable the generation of 3D cell culture structures like spheroids or organoids. Such cultures are becoming increasingly common in preclinical research, as they reflect the physiological properties of cells much better than monolayer cell cultures [1, 4].

Immunoassays combined with 3D confocal microscopy are essential tools for the analysis of cell cultures models on single cell level. Immunostainings with fluorescent markers enable the spatio-temporal visualization of specific cell structures such as proteins or nucleic acids, which allows, for example, metabolic or morphological changes to be detected after treatments.

Multiple immunostaining technique is a combination of individual antigen detections in order to study the expression and co-localization of two or more different antigens in the same sample. However, the number of spectral profiles and the wavelengths of absorbance and emission of fluorescent dyes is limited, which restricts the available number of markers that can be used simultaneously.

In cases where such incompatibilities occur, additional cell culture samples are often prepared in which the incompatible markers are exchanged. This introduces additional effort and costs. Additionally, as the markers are divided among different samples, direct correlations between them can no longer be analyzed. Furthermore, some markers also have a negative impact on the cell cultures and can thus influence the results.

In the medical imaging field, methods have been published which transform images of one modality like MRT into another modality like CT [9, 13, 14]. In the biological field, Christiansen et al. [3] and Ounkomol et al. [10] used a deep learning model to predict fluorescent labels based on unstained transmitted light images in 2D and 3D respectively. The two methods can be considered as filter methods since the structures to be predicted are contained in the transmitted light image. Rivenson et al. [11] used a deep learning model to predict a stained bright-field image based on the auto-fluorescence of an unstained sample.

In contrast to the above mentioned approaches, we introduce a method to predict additional fluorescent labels based on a nuclei staining (Draq5), imaged with a confocal microscope. In this case, the nuclei staining does not contain direct information about the signal to be predicted. Only the morphological features of the nuclei and its texture can be used. Furthermore we use 3D spheroid cell cultures with a diameter of up to 400 µm. Such recordings suffer from a reduced brightness and quality in deeper regions and therefore provide an additional challenge for the transformation.

*Corresponding author: Roman Bruch,** Institute for Automation and Applied Informatics, Karlsruhe Institute of Technology, Eggenstein-Leopoldshafen, Germany, e-mail: roman.bruch@kit.edu
Mario Vitacolonna, Rüdiger Rudolf, Center for Mass Spectrometry and Optical Spectroscopy (CeMOS) and Institute of Molecular and Cell Biology, Mannheim University of Applied Sciences, Mannheim, Germany
Markus Reischl, Institute for Automation and Applied Informatics, Karlsruhe Institute of Technology, Eggenstein-Leopoldshafen, Germany

The presented method is based on a deep learning model. We introduce a workflow to measure the performance of our model and analyze the impact of a potential signal bleed through using Ki67, a cellular proliferation marker.

2 Methods and Data

Our goal is to predict additional fluorescent labels based on a nuclei staining. For this task we use a 3D version of a deep residual U-Net (3D ResUnet), a combination of the widely established U-Net [12] and deep residual network [6]. To train this model, paired training data is needed. E.g. the positions of the underlying structures need to match between the two stainings. This is easily achieved by staining cell cultures with the nuclei and the marker to predict. Afterwards, both stainings are recorded in a normal fashion. The network is then trained to minimize the difference between its prediction and the real staining. During inference images only stained with the nuclei marker can be used.

The 3D ResUnet used is based on the 3D U-Net [2]. The two convolutions in each block of the downsampling path are replaced by a residual block [6]. Each residual block is preceded by an additional convolution. Furthermore batch normalization layers are added after ReLu activation functions and transposed convolutions.

The mean squared error (MSE) between the predicted voxels and the ground truth was used as loss function. Training was performed with a learning rate of 0.001, the lookahead optimizer and a batch size of two. The training was continued until the validation loss did not improve for 20 consecutive iterations. The model state with the best validation score was selected as the final model.

The data used for training and evaluation was recorded with a confocal microscope. In this work we focused only on the prediction of a Ki67, a marker for cellular proliferation. The nuclei marker used in this study is Draq5. As cell culture models, mono-culture spheroids with A549 and KP4 cells and co-culture spheroids with additional fibroblasts were used. The 3D images were recorded with a voxel size of $1 \times 0.568 \times 0.568$ µm (z,y,x). Fig.1 shows an exemplary image of a 3D spheroid.

As the GPU memory was limited, the images were sliced into patches with size $32 \times 128 \times 128 px^3$ before training. 2265 patches resulting from 20 images stained with Draq5 and Ki67 were used as training data. For validation, 1161 patches resulting from 10 images were used. The evaluations described below were performed with additional test data.

To test the performance of the trained network, the Pearson correlation coefficient between the predicted and the real
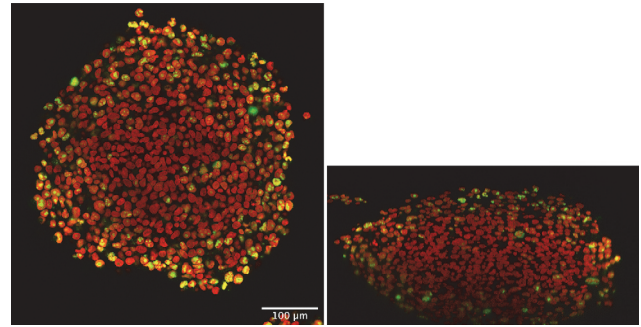
Fig. 1: An exemplary xy-slice (left) and xz-slice (right) of a 3D spheroid. Nuclei and Ki67 stainings are shown in red and green, respectively. Scale bar: 100 µm.

Ki67 staining was calculated. This was done on both, voxel and object scale levels with a total number of nine spheroids. For calculating the correlation coefficient on the voxel scale level, only voxels located inside the nuclei were used. Since most of the Ki67 signal was expressed inside the nuclei, the regions outside appeared mostly black and therefore easy to predict. The object based correlation coefficient was calculated by using the mean intensity of single nuclei. The nuclei regions were calculated by a 3D instance segmentation of the nuclei channel.

To test whether the model is affected by cross talk from the real Ki67 staining into the nuclei staining, additional spheroids were stained with Caspase 3 instead of Ki67. Importantly, both signals were imaged at a similar wavelength range, but were distributed in completely different locations inside the cells. If the model relied on cross talk signal, the predicted Ki67 should be similar to the Caspase signal. Since ground truth was no longer available in this case, only the correlation between the predicted Ki67 and the Caspase signal was analyzed. In addition a visual comparison was presented.

Another pertinent readout from fluorescence images was the number of positive cells/nuclei based on a stained label. To see how well the predicted Ki67 staining was suitable to extract this information, we used a support vector machine classification model to determine the number of Ki67 positive nuclei. This model uses on the mean intensity of the nuclei and Ki67 signal in and around the nuclei. The model is trained only on real stainings of Ki67. The trained model is then applied to an image of a spheroid with real and predicted Ki67 staining.

3 Results

The results of the Pearson correlation test are shown in Fig.2. For the voxel based analysis the median correlation coefficient between real and predicted Ki67 staining was 0.687. The cor-
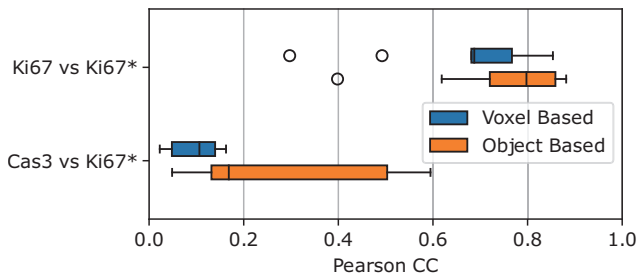
Fig. 2: Pearson correlation coefficient between real and predicted Ki67 and between real Caspase 3 and predicted Ki67. Both are shown for a voxel based level (only foreground) and an object based level.
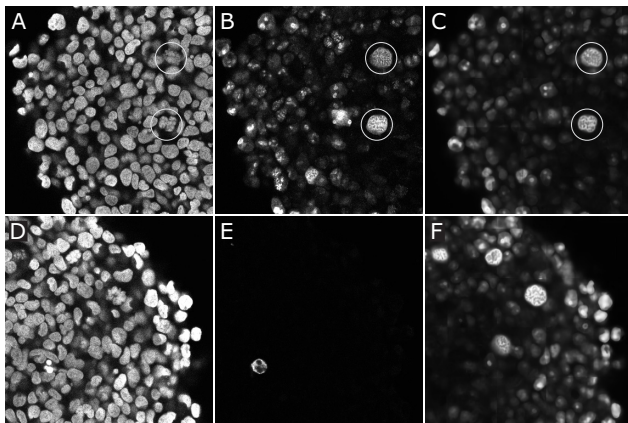
Fig. 3: Spheroid stained with a nuclei marker (A) and Ki67 (B). The predicted Ki67 signal is shown in (C). Spheroid stained with a nuclei marker (D) and Caspase 3 (E) represents an application example for the presented method. The prediction of the Ki67 staining is shown in (F).

responding median value for the object based analysis was higher (0.798), but the data showed a greater variation. For the spheroids stained for Caspase 3 instead of Ki67, the median correlation coefficient between real Caspase 3 and predicted Ki67 was 0.12 and 0.167 the voxel and object based analysis, respectively.

Fig.3 allows a visual inspection of the predicted Ki67 signal. The figure shows zoomed image slices of two spheroids. The first was stained with the nuclei (A) and Ki67 (B) marker. The predicted Ki67 staining is shown in (C). Notably, there was a large similarity between real and predicted data. However, while in the image of the real Ki67 staining, fine structures much smaller than the nuclei are visible, the predicted staining mostly misses this granularity and appears more blurred. Interestingly the prediction model was able to replicate the increased area of the Ki67 signal compared to the nuclei for the cells in the mitotic state (white circles). The other spheroid was stained for nuclei (D) and Caspase 3 (E). The prediction of the Ki67 staining for this spheroid is shown in

(F). The predicted Ki67 staining shows no similarity to the Caspase 3 signal. Instead, the prediction looked similar to the one given in (C). One can see, that the mitotic cells in the top right share a similar predicted Ki67 signal compared to the previous images.

In the following, the classification results of the real and predicted Ki67 staining are presented. In total the model assigned 91% of 19625 nuclei to the same class. The F1 score between the two results was 0.84 and the number of false positive and false negative errors was rather similar with 783 (4%) and 931 (5%).

4 Discussion

As Fig.2 shows, the median correlation coefficient between real and predicted Ki67 signal was higher in the object based analysis than in the voxel based analysis. This was expected, as noise present in the real signal can not be predicted by the model and thus has a worsening effect on the result. As can be seen in Fig.3, the predicted staining appeared more blurred, which further increased the intensity differences between the voxel pairs.

The blurry prediction was an effect of using the mean squared error loss for network training [8]. As Isola et al. [7] proposed, the sharpness may be increased by using a generative adversarial network (GAN) training strategy with a Patch-GAN discriminator. However, this leads to additional overhead, increasing training time and memory consumption.

As can be seen in Fig.3, the prediction of the Ki67 staining seemed to work well for cells in the mitotic state (white circles). Here, the model was even able to mimic the texture of the staining. It should be noted, that the nuclei in this state have a distinct shape and texture which can easily be recognized by the model. The model failed, however, at the fine structures in the signal. These either are combined into a blurry representation, or are completely missing in the prediction. A solution for this could be training and inference of the model on a higher image resolution.

As the image was too large to be processed in one run, it was split into multiple patches. After processing, the patches were combined to form the complete image. But as can be seen in Fig.3, the procedure can lead to visible transition artifacts. It is expected that advanced tiling and merging strategies as used in [5] will greatly improve this.

Based on the image of the spheroid stained for Caspase instead of Ki67 (see Fig.3 second row) it can be assumed that the model is not relying on signal cross talk between the channels. The increased brightness in (F) compared to (C) might be explained by the higher intensity in the nuclei image. Also as

shown in Fig.2 the median correlation between Caspase 3 and the predicted Ki67 signal is weak. In summary, it appears that the proposed training method can thus be used without major drawbacks in a later inference state, where no Ki67 is stained or other markers are stained.

Furthermore, as the results of the classification analysis have shown, the predicted signal can be used with an existing classification model with a small trade off in accuracy. This may allow a combined use of real and synthetic stainings in such an analysis.

5 Conclusion

In this work we introduced a method for the synthesis of fluorescent stainings based on a nuclei staining. On a nuclei scale level, a median correlation coefficient of 0.798 was achieved. We showed, that an existing analysis method can also be used with predicted Ki67 stainings. We furthermore demonstrated that the performance of the model is not a result of potential signal bleed through.

For the method to work with other stainings, information such as distinct morphologies or textures, corresponding to what the marker is targeted to, need to be present in the nuclei channel. The information can also be more complex like the brightness compared to the size of a nucleus. Suitable would be, for example, markers for cell apoptosis, cell cycle stages, metastatic cells or cell type classification. Such markers could potentially be completely replaced by their synthetic counterpart, accelerating the preparation and imaging time. However, this needs to be tested in future experiments. Additionally, we want to test the prediction of markers expressed in the cytoplasm outside the nuclei region.

To allow for a quantitative bleed through analysis, we further plan to perform a two-step staining, where first the nuclei marker and then the Ki67 marker are stained and imaged. We will also evaluate, if the use of a PatchGAN discriminator will improve the sharpness of predicted structures.

References

[1] Alépée N. State-of-the-art of 3d cultures (organs-on-a-chip) in safety testing and pathophysiology. *ALTEX* 2014;31:441–477.

[2] Çiçek O, et al. 3D U-Net: Learning dense volumetric segmentation from sparse annotation. In: Medical Image Computing and Computer-Assisted Intervention – MICCAI Springer International Publishing 2016, 424–432.

[3] Christiansen EM, et al. In silico labeling: Predicting fluorescent labels in unlabeled images. *Cell* 2018;173:792–803.e19.

[4] Drost J, et al. Organoids in cancer research. *Nature Reviews Cancer* 2018;18:407–418.

[5] Eschweiler D, et al. 3d fluorescence microscopy data synthesis for segmentation and benchmarking. *PLOS ONE* 2021;16:e0260509.

[6] He K, et al. Deep residual learning for image recognition. In: Proceedings of the IEEE conference on computer vision and pattern recognition. 2016, 770–778.

[7] Isola P, et al. Image-to-image translation with conditional adversarial networks. In: Proceedings of the IEEE conference on computer vision and pattern recognition. 2017, 1125–1134.

[8] Larsen ABL, et al. Autoencoding beyond pixels using a learned similarity metric. In: Proceedings of The 33rd International Conference on Machine Learning, volume 48 of *Proceedings of Machine Learning Research* PMLR, New York 2016, 1558–1566.

[9] Nie D, et al. Medical image synthesis with context-aware generative adversarial networks. In: International conference on medical image computing and computer-assisted intervention Springer 2017, 417–425.

[10] Ounkomol C, et al. Label-free prediction of three-dimensional fluorescence images from transmitted-light microscopy. *Nature Methods* 2018;15:917–920.

[11] Rivenson Y, et al. Deep learning-based virtual histology staining using auto-fluorescence of label-free tissue. *arXiv preprint arXiv:180311293* 2018;.

[12] Ronneberger O, et al. U-Net: Convolutional networks for biomedical image segmentation. In: Lecture Notes in Computer Science Springer International Publishing 2015, 234–241.

[13] Vemulapalli R, et al. Unsupervised cross-modal synthesis of subject-specific scans. In: Proceedings of the IEEE International Conference on Computer Vision. 2015, 630–638.

[14] Xiang L, et al. Deep auto-context convolutional neural networks for standard-dose pet image estimation from low-dose pet/mri. *Neurocomputing* 2017;267:406–416.